Author Manuscript

Author Manuscript

Author Manuscript

Author Manuscript

HHS Public Access

Author manuscript

Aerosol Sci Technol. Author manuscript; available in PMC 2020 August 06.

Published in final edited form as:

Aerosol Sci Technol. 2018 ; 52(11): 1233–1248. doi:10.1080/02786826.2018.1513636.

Aerosol size distribution measurement of electronic cigarette emissions using combined differential mobility and inertial impaction methods: Smoking machine and puff topography influence

Vladimir B. Mikheev[a], **Alexander Ivanov**[a], **Eric A. Lucas**[a], **Patrick L. South**[a], **Hendrik O. Colijn**[b], **Pamela I. Clark**[c]

[a]Battelle Memorial Institute, Columbus, Ohio, USA

[b]Center for Electron Microscopy and Analysis, Ohio State University, Columbus, Ohio, USA

[c]University of Maryland, College Park, Maryland, USA

Abstract

A combination of a real-time high resolution aerosol differential mobility spectrometer (DMS500) and an electrical low pressure impactor (used as a traditional impactor) was applied to simultaneously collect real-time data and analyze particle size by weighing the mass of the aerosol collected on the impactor stages. Nonrefillable fixed-power as well as refillable and power adjustable e-cigarettes (e-cigs) were tested at various puffing flow rates. Two types of smoking machines were used: a smoke cycle simulator that provides instantaneous straight sample delivery to the analyzer and a Human Profile Pump that utilizes two synchronized pistons and operates by sample pull–push mode. Chemical analysis of the major components of e-liquid (propylene glycol, vegetable glycerol, water, and nicotine) was made using a proton nuclear magnetic resonance method. Limited amounts of samples collected on impactor stages were analyzed by liquid chromatography time-of-flight mass-spectrometry to find newly formed semi- or low-volatile organic compounds in e-cig aerosol and by transmission electron microscopy to check for the presence of nanoparticles in e-cig emissions. Differential mobility and inertial impaction methods showed comparable particle size results. Method of aerosol generation (type of the smoking machine) as well as puffing topography affected the e-cig particle size. Newly formed semi- or low-volatile organic compounds as well as metal nanoparticles were found in e-cig aerosol.

Introduction

E-cigarette (e-cig) popularity is growing worldwide and in particular among adolescents (Delnevo et al. 2015; Singh et al. 2016). There is a perception about the relative safety of e-

Full Terms & Conditions of access and use can be found at https://www.tandfonline.com/action/journalInformation?journalCode=uast20

CONTACT Vladimir B. Mikheev, mikheevv@battelle.org, Public Health Center for Tobacco Research, Battelle Memorial Institute, 505 King Avenue, Columbus, OH 43201, USA.

Color versions of one or more of the figures in the article can be found online at www.tandfonline.com/uast.

Supplemental data for this article is available online at https://doi.org/10.1080/02786826.2018.1513636

Author Manuscript Author Manuscript Author Manuscript Author Manuscript

cigs based on their comparison with traditional combustible cigarettes (Volesky et al. 2016). Although the level of some toxic constituents such as aldehydes (Bekki et al. 2014; Goniewicz et al. 2014; Hutzler et al. 2014; Kosmider et al. 2014; Tayyarah and Long 2014; Jensen et al. 2015; Geiss, Bianchi, and Barrero-Moreno 2016; Khlystov and Samburova 2016; Sleiman et al. 2016; Ogunwale et al. 2017), metals (Williams et al. 2013; Lerner et al. 2015; Mikheev et al. 2016), and free radicals (Lerner et al. 2015) normally either do not dramatically exceed or are often even lower in e-cig emissions than in traditional cigarettes, and well known tobacco specific nitrosamines (TSNAs) carcinogens may not be presented in e-cigs emissions at all (Farsalinos et al. 2015), it does not provide full evidence that e-cigs could be used as a safer alternative to combustible cigarettes.

While assessing the potential harmful effects of e-cigs it should be noted that e-cigs do not burn tobacco but instead use a resistively heated wire placed in direct contact with an e-liquid mixture of propylene glycol (PG), vegetable glycerol (VG), nicotine, water, and flavorants. Heating this organic liquid mixture in the presence of oxygen on a metal catalytic surface (Rossiter Jr et al. 1985; Tuma et al. 2013; Saliba et al. 2018) results in chemical transformations that produce a number of compounds that were not originally present in the e-liquid (Bekki et al. 2014; Goniewicz et al. 2014; Hutzler et al. 2014; Kosmider et al. 2014; Tayyarah and Long 2014; Jensen et al. 2015; Geiss, Bianchi, and Barrero-Moreno 2016; Khlystov and Samburova 2016; Sleiman et al. 2016; Jensen, Strongin, and Peyton 2017; Ogunwale et al. 2017; Salamanca et al. 2017; Korzun et al. 2018). Some of these newly formed compounds such as aldehydes (Bekki et al. 2014; Goniewicz et al. 2014; Hutzler et al. 2014; Kosmider et al. 2014; Tayyarah and Long 2014; Jensen et al. 2015; Geiss, Bianchi, and Barrero-Moreno 2016; Khlystov and Samburova 2016; Sleiman et al. 2016; Ogunwale et al. 2017) are similar to those found in traditional tobacco smoke but compounds such as acetol and glycidol, formaldehyde hemiacetals, and dihydroxyacetone—derivatives from heated VG and PG are inherent to e-cig emissions (Jensen, Strongin, and Peyton 2017; Salamanca et al. 2017; Korzun et al. 2018; Vreeke et al. 2018).

The problem of accurate e-cig toxicity assessment becomes even more complicated since along with respiratory tract geometry and respiratory parameters aerosol delivery/deposition efficiency in the human respiratory tract strongly depends upon aerosol particle size, which is not easy to measure given the presence of relatively volatile and volatile compounds (PG and water), and also the hygroscopic properties of both PG and VG (main components of e-liquid). E-cig aerosol may either quickly evaporate (if strongly diluted), absorb water in a humid environment, or grow and coagulate (if provided enough residence time). A clinical trial (St. Helen et al. 2016) showed that unlike combustible tobacco smoke e-cig aerosol delivered a significant amount of nicotine to sites other than the lungs (probably buccal mucosa and gastrointestinal tract following swallowing), which may indicate either larger particles (that were not able to penetrate the lungs) or the significant presence of nicotine in a vapor phase (that was deposited via diffusion before reaching the lungs). An ideal device to measure e-cig aerosol size should have real-time capability (to monitor quick changes in the dynamics of aerosol formation during puff development), provide quick sample delivery to analysis under minimal or no dilution (to avoid evaporation or coagulation), cover high particle concentrations (up to 10^9 particles/cc), and wide size distributions (nm to microns). Currently, there is no single instrument that could satisfy all these requirements: therefore, a

Author Manuscript Author Manuscript Author Manuscript Author Manuscript

combination of techniques has to be used to obtain accurate measurements of e-cigs aerosol size. Several approaches exploiting different experimental techniques were applied including optical transmission (Ingebrethsen, Cole, and Alderman 2012) and laser scattering (Cabot et al. 2013; Pratte, Cosandey, and Goujon-Ginglinger 2016; Dunkhorst et al. 2018), differential (electrical) mobility real-time (Ingebrethsen, Cole, and Alderman 2012; Fuoco et al. 2014; Marini et al. 2014; Manigrasso et al. 2015; Mikheev et al. 2016; Baassiri et al. 2017; Scungio, Stabile, and Buonanno 2018) and scanning mobility near real-time (Zhang, Sumner, and Chen 2013; Fuoco et al. 2014; Zhao et al. 2016) methods, and inertial impaction (Alderman et al. 2015; Baassiri et al. 2017; Oldham et al. 2018).

Each of these techniques has both advantages and limitations. Optical techniques are real-time, have high particle size resolution, can measure large particles (up to 2,000 microns), and may work with no sample dilution unless particle concentrations reach ~10^9 per cm^3 as was reported for e-cigs (Ingebrethsen, Cole, and Alderman 2012) at which point coincidence counting and cloud behavior start to affect the measurements (Fuchs 1964; Hinds 1982; Martonen 1992; Phalen, Oldham, and Schum 2002). Another disadvantage is that with a lower size limit (~100 nm) optical techniques can't measure small particles, and the measurement results are interpreted based on a log-normal distribution assumption and therefore do not cover bi-modal (or more complicated) types of size distributions. Use of the refractive index to calculate particle size distribution may also affect optical measurement accuracy due to the dynamic nature of e-cig aerosol (continuous aerosol-vapor phase exchange of the main components such as PG, VG, and water). Advanced electrical mobility methods are also real-time and have high particle size resolution but require some sample dilution (therefore partial evaporation is possible). Electrical mobility methods are capable of reaching down to the nanometer size range (2.5–5 nm) although their upper particle size limit is normally restricted to 1 micron (2.5 micron is the highest available upper limit). Inertial impactors are not real-time techniques and do not have high particle size resolution. Sample dilution might be avoided or minimized but that would require special design features to match the impactor sampling flow rate. The upper particle size limit is normally about 10 microns and the lower size limit of the advanced impactors is ~17–18 nm.

Because of these technical complications associated with e-cig aerosol size measurements it becomes critically important to compare results obtained using different measurement principles from the same type of e-cigs vaped under the same conditions. That would allow the elimination of possible experimental artifacts caused by the limitations from any of the methods described above. Unfortunately, due to numerous factors such as methods of aerosol generation (type of smoking machine used), sample processing difference (including dilution or even thermal dilution), types of e-cigs and e-liquids, and differences in puffing topography, an accurate direct comparison of the published results is not possible in most cases. Only two studies (Ingebrethsen, Cole, and Alderman 2012; Alderman et al. 2015) applied different methods (spectral transmission vs inertial impaction) using similar puffing topography (50 and 55 mL/s puff flow rates at 3 s duration) to measure particle sizes of the undiluted mainstream aerosol of the same two brands of e-cigs (with the known chemical content of e-liquid for one of the brands). One of the brands tested (with unknown e-liquid chemical content) showed very similar count median diameters (CMDs), 261 vs 265 nm, measured by impactor vs spectral transmission respectively. Another brand (with

Author Manuscript Author Manuscript Author Manuscript Author Manuscript

approximately 50/50 PG/VG e-liquid content) showed CMD of 262 vs 339 nm (impactor vs spectral transmission). Differences were also observed for gravimetric data measured from aerosol mass collected on the filter (3.07 vs 4.1 mg/puff). An explanation of these results is complicated since differences could be attributed to a number of reasons: partial evaporation of PG (and water), similar but not equal puffing flow rate, possible difference between e-cigs tested (even from the same brand), and finally experimental artifacts caused by the different measurement principles applied.

It becomes clear from this analysis that to obtain and compare independent data of e-cig aerosol size using two different methods, simultaneous measurements from the same e-cig (with known e-liquid content) vaped under a controlled puffing topography are required. Therefore, the first goal of this study was to design an experimental setup to compare e-cig aerosol size measurements made by two widely used and well recognized techniques: electrical mobility and inertial impaction. Also, taking into account all inherent e-cig aerosol measurement complications discussed above we've tried to identify the most critically important tests that have to be conducted to clarify important questions about e-cig operational properties and methods of measurements that are not yet fully answered.

An e-cig is an aerosol generator that works as follows: first the e-liquid impregnates a wick (that is wrapped by a heating coil), then the wick is heated vaporizing the e-liquid, and simultaneously air is pulled through the heated zone. Air becomes saturated with e-liquid vapor and then enters the delivery channel where quick cooling creates supersaturation conditions (supersaturation is defined as a ratio of the actual vapor concentration to the equilibrium vapor concentration at given temperature). Once vapor reaches a critical supersaturation level then homogeneous nucleation starts resulting in a new aerosol formation (Stauffer 1976; Oxtoby 1992). This process has been investigated in detail using the laminar flow tube reactor (flow diffusion cloud chambers) by a number of studies (Hämeri et al. 1996; Vohra and Heist 1996; Mikheev et al. 2000, 2002) where precise control over the temperature at each section of the flow chamber as well as controlled vapor concentration were provided. Nucleation (aerosol formation) rate is an exponential function of temperature and supersaturation (Oxtoby 1992) therefore any shift of these parameters causes a drastic change in aerosol concentration. Puffing flow rate increases on one hand may carry more vapor from the wick to the nucleation zone and therefore enhance aerosol formation, but at some point should cause e-liquid exhaustion from the wick as well as a cooling effect on the heated coil and both factors will result in an aerosol formation rate decrease. An increase of the puffing flow rate also results in a decrease of the aerosol growth time and consequently particle size may also decrease. Therefore, determining the influence of the puffing flow rate on the aerosol size and concentration was the second goal of this study.

Due to the extreme sensitivity of e-cig aerosol/vapor to a residence time it is also of a critical importance to understand how a piston pull–push based smoking machine may affect aerosol size in comparison with the smoking machine that provides direct smoke delivery from the e-cig outlet to analysis. A recent study measured highly diluted (1/10,000) e-cig aerosol using laser optical scattering (Pratte, Cosandey, and Goujon-Ginglinger 2016) and showed that applying a piston pull–push approach (increasing aerosol residence time by ~3.4 s) led

Author Manuscript Author Manuscript Author Manuscript Author Manuscript

to a moderate particle size increase in comparison with direct push aerosol method for analysis. More studies are required to analyze the effect of residence time at low sample dilution and using alternative aerosol size measurements techniques, therefore a study of the influence of different types of the smoking machines on the particle size distribution was the third goal of this study.

Materials and methods

Electronic cigarettes tested, smoking (vaping) machines used, and puff topography parameters applied

The study used nonrefillable blu e-cigs (purchased in 2014–2016) at mid-nicotine strength (6–9 mg/mL) and six flavors: classic tobacco (CT), magnificent menthol (MM), cherry crush (CC), peach schnapps (PS), pina colada (PC), and vivid vanilla (VV). In addition, two types of the refillable e-cigs with adjustable heating power (Figure S1) were also investigated: a cylindrical shaped iTaste SVD (operated at 5 V and 1.8 ohm heating element resistance) and a box shaped iTaste VTR (operated at 4 V and 2.1 ohm heating element resistance). A 50/50 mixture of PG/VG solution was used for the refillable e-cigs tests.

Two types of smoking (vaping machines) were used: Smoke Cycle Simulator (SCS, Cambustion Ltd, Cambridge, UK) which provides instantaneous sample delivery for analysis and the Human Profile Pump (HPP2, CH Technologies, Westwood, NJ, USA) which operates in a piston pull–push sample fashion. Both machines can operate under user specified puff profiles by downloading Excel-type (or similar) files that contains flow rate (mL/s) vs time (20 ms increments) data columns, providing user defined puffing topography. This study applied square type puff profiles, at 5 s puff duration, and at various flow rates (from 15 to 45 mL/s) at 60 s inter-puff intervals.

Aerosol particle size distribution characterization

The Differential Mobility Spectrometer (DMS500, Cambustion Ltd, Cambridge, UK) in combination with Electrical Low Pressure Impactor (ELPI+, Dekati Ltd, Kangasala, Finland) were used to measure aerosol size distribution in real-time (via DMS500) and simultaneously collecting samples on ELPI + stages for gravimetric analysis (Figure 1). DMS500 allows for real-time (0.1 s response time) measurements at high particle size resolution (38 size classes) within wide particle size and concentration ranges (5 nm to 1 μm, and up to 9 orders of magnitude, respectively) at high and low sample dilution. ELPI + is capable of real-time measurements in 14 size fractions (6 nm to 10 μm) but due to concentration limitations operating in a real-time fashion requires high dilution that could seriously affect the aerosol size measurements of e-cig emissions. Therefore ELPI + was used for gravimetric analysis only as a standard impactor by collecting aerosol on aluminum foils placed on the impactor stages.

E-cig aerosol generated by either SCS or HPP2 was additionally diluted by 20 L/min of HEPA filtered air-flow (to provide enough sample for both devices and prevent oversaturation of the DMS500 electrometers) and then the sample flow was split into two lines for the simultaneous DMS500 and ELPI + measurements. ELPI + requires a constant

Author Manuscript Author Manuscript Author Manuscript Author Manuscript

10 L/min flow whereas the DMS500 was set to a 40 L/min sampling flow rate (8 L/min to the classifier column and 32 L/min were exhausted). Under these conditions at a 25 mL/s (1.5 L/min) flow rate through the e-cig the SCS adds 28.5 L/min of dilution bringing the total sample flow to 50 L/min and overall dilution to a factor of 1.5/(1.5 + 28.5) × 30/(30 + 20) = 1/33. While using the HPP2 piston pull and push speeds were set to the same 25 mL/s (1.5 L/min) flow rate and an additional 28.5 L/min of HEPA filtered air was provided to the HPP2 pushed flow therefore making the total dilution factor the same as for the SCS 1/33. DMS500 settings were adjusted (in coordination with the instrument manufacturer) so calculations of the aerosol concentration made by the DMS500 software took into consideration the part of the sampling flow that was directed to the ELPI+. DMS500 software provided particle number concentration, CMD, and geometrical standard deviation (GSD) measurements (at user selected size ranges). ELPI + stages were individually weighed and used for mass median aerodynamic diameter (MMAD) determination. CMD data obtained by DMS500 were recalculated to mass median diameter (MMD) using the Hatch-Choate equation (Hatch and Choate 1929) then converted to MMAD (Hinds 1982) and compared with ELPI + data. An additional set of measurements using the DMS500-SCS setup (no ELPI + or HPP2 measurements were involved) was conducted for the blu e-cigs with varying puffing flow rates at 15, 25, 35, and 45 mL/s. Particle number concentration and CMD were compared for the two size ranges: from 5 to 40 nm and from 41 to 1,000 nm.

Total aerosol (particulate) mass (TPM) collected from all ELPI + stages was measured for all blu e-cigs tested. TPM was also collected on the Cambridge glass-fiber 47 mm filters from the blu e-cig (CT flavor, three replicates vaped) using both smoking machines (SCC and HPP2) under the same puffing topography (as was used for DMS500 and ELPI + samples collection). Total aerosol mass outcome mg/puff was defined for both ELPI + and filter collected samples.

In addition, to check evaporative properties of e-cig aerosol at high sample dilution a rotating disk dilution option (1/500 dilution ratio) was activated in DMS500 similarly to our previous study (Mikheev et al. 2016) and aerosol generated by both SCS and HPP2 smoking machines was measured at high dilution conditions.

E-liquid analysis

E-liquid analysis for the major component (PG, VG, nicotine, and water) of blu e-cigs was conducted using the proton nuclear magnetic resonance (HNMR) method described elsewhere (Crenshaw et al. 2016). E-liquid was extracted from the cartridges by 15 min of centrifuging at 3,000 revolutions per minute (~1–2 mL/cartridge). An accurately weighed 100 μL aliquot of each e-liquid was dissolved in an accurately weighed aliquot of a solution prepared by dissolving an accurately weighed amount of internal standard (maleic acid) in an accurately weighed amount of dimethylsulfoxide-d6 (DMSO-d6) to provide a concentration of approximately 30 mg/mL of internal standard. The HNMR analysis was conducted using a Bruker Advance 500 FT-NMR spectrometer with an operating field of 11.75 T.

Author Manuscript Author Manuscript Author Manuscript Author Manuscript

Analysis of the samples collected on ELPI foils

A limited amount of samples (blu e-cigs CC and PC flavors at mid-nicotine strength) were analyzed by a liquid chromatography time-of-flight-mass-spectrometry (LC-TOFMS) method to check for the presence of the newly formed semi- or low-volatile organic compounds in e-cig aerosol and by transmission electron microscopy/scanning transmission electron microscopy (TEM/STEM) to check for the presence of nanoparticles in e-cig emissions. Aerosol samples were collected on aluminum foils placed on the ELPI stages (40 puffs at 25 mL/s flow rate per each test were used). Blank air samples (of the laboratory air) were collected using the same amount of puffs and same puffing flow rate and subtracted from the analysis. ELPI foils were heated to 450 °C for a minimum of 8 h in a muffle oven and then stored in an airtight container until needed for use. Foils were loaded onto the ELPI stages and were transferred to petri slides immediately after the sample collection was complete. Foils transferred for LC-TOFMS testing were stored in previously muffled Fisher Scientific brand 30 mL straight sided jars in a −20 °C freezer until ready for analysis. Samples sent for TEM/STEM analysis were stored in the petri slides at room temperature until ready for analysis.

LC-TOFMS analysis—Aerosol samples collected on ELPI foils as well as e-liquid extracted from the cartridges (by the procedure described in the previous section) were analyzed using LC-TOFMS to detect if any new low- (or semi-) volatile organic compounds were formed as a result of catalytic heating of e-liquid during vaporization. The foils were fortified with an internal standard solution and successively extracted three times by sonication with 50:50 dichloromethane:acetonitrile. The extracts were combined and concentrated by Kuderna–Danish to 1 mL. An aliquot (100 μL) of the concentrated extract was evaporated to dryness under nitrogen, and the residue was reconstituted in 100 μL of 100 mM aqueous ammonium acetate for analysis. The analytical method consisted of a reversed-phase gradient HPLC separation followed by high resolution time-of-flight (TOF) analysis using TurboIonSpray (electrospray) in positive mode. The acquisition method consisted of both a TOF-MS scan (full-scan screen) and Information Dependent Acquisition (IDA) product ion scans of computer-selected precursor ions. The mass spectrometer signal intensities were plotted versus time to yield ion chromatograms. The spectrometer was mass-calibrated before the start of the sequence by infusing Sciex Tuning Solution through the TurboIonSpray probe, and then was re-calibrated throughout the batch by infusing Sciex APCI Positive Ion Calibration Solution through the APCI probe. The Enhanced Peak Find algorithm was also employed on the raw data to detect non-targeted peaks in the test samples. The data were searched against commercial drug, pesticide, and metabolite spectral libraries. Supporting evidence was provided by using the instrument software tools designed to assign molecular formulae (Formula Finder). Further details of the instrument operation could be found in Table S1.

TEM/STEM analysis—To detect nanoparticles the aerosol collected on ELPI foils was analyzed by an FEI Tecnai F20 TEM/STEM equipped with an EDAX 30 mm^2 windowless Energy Dispersive Spectroscopy (EDX) detector using a recently developed method (Colijn et al. 2018). Prior to analysis the condensed glycerol and PG was evaporated from the aluminum foils by heating overnight over an incandescent lamp. Samples were transferred

Author Manuscript Author Manuscript Author Manuscript Author Manuscript

on TEM grids by using a modified TEM replica method. A thin cellulose acetate tape softened with acetone was placed on the foil, gently pressed onto the surface, and allowed to dry. The tape with particles was then carbon coated and the cellulose acetate tape dissolved. The carbon film with particles was then examined in the TEM/STEM using High Angle Annular Dark Field (HAADF) imaging as well as conventional TEM imaging.

Results

Aerosol size distribution: Puffing flow rate influence

Results of the puffing flow rate influence on aerosol size and concentration for all six flavors of blu e-cigs are presented at Figure 2. Similar data collected for the two refillable and power adjustable e-cigs (iTaste SVD and iTaste VTR) are presented at Figure 3. Data were obtained using the DMS500 for the two particle size ranges: 5–40 nm and 41–1,000 nm. These two particle size ranges were chosen based on analysis of the aerosol size distribution to separate log-normally distributed particles of the submicron range (41–1,000 nm) from the more complicated spectrum of the nanoparticles (5–40 nm) as it could be seen from Figures 4–6 (and Figures S2–S4) where aerosol spectrums are presented for all tested flow rates (for all types of e-cigs tested).

All blu e-cigs demonstrated a similar trend: at a low flow rate (15 mL/s) the concentration of nanoparticles was always lower than the submicron particles. The concentration of the submicron particles increased when the flow rate grew from 15 to 35 mL/s and either stabilized or started to decrease at a 45 mL/s flow rate. The concentration of nanoparticles steadily increased while the flow rate grew from 15 to 45 mL/s and reached the level of the submicron particles. CMD was steadily decreasing for the submicron fraction and stayed stable for the nanoparticles while the flow rate was growing.

The refillable iTaste SVD e-cig, similarly to the blu e-cigs, showed lower nanoparticle concentrations at a 15 mL/s flow rate and then both nanoparticles and submicron particle concentrations increased, but nanoparticles were still lower than the submicron particles at high flow rates (Figure 3). The iTaste VTR e-cig showed the same level of nanoparticles and submicron particles at low flow rates, then nanoparticle amounts increased as flow rate increased and stabilized at 35 and 45 mL/s whereas submicron particle concentrations increased at a 25 mL/s flow rate and demonstrated decrease when the flow rate was further increased (Figure 3). CMD for both refillable e-cigs showed a trend similar to blu e-cigs—steady decrease of submicron particle CMD with the flow rate growth and stable nanoparticle CMD across the entire range of flow rates (Figure 3).

Aerosol size distribution: DMS500 vs ELPI and SCS vs HPP2

Results of the DMS500 measurements obtained using SCS (CMD and calculated MMAD) as well as a comparison with ELPI measured MMAD (also obtained from the SCS aerosol generation) are summarized in Table 1. To calculate MMD the Hatch–Choate equation (Hatch and Choate 1929) was applied for the log-normally distributed submicron mode of the aerosol size spectrum (mass of the nano-fraction was ~0.1% of the submicron fraction therefore the nano-fraction can be ignored for the purpose of MMD calculations), and then

Author Manuscript Author Manuscript Author Manuscript Author Manuscript

MMD was converted to MMAD (Hinds 1982) by multiplying to the square root of the particles density (assuming the 50/50 PG/VG mixture would have average density of 1.15 g/cm^3). The data were collected at 25 mL/s puffing flow rate with a 5 s puff duration using 40 puffs and 1 min inter-puff interval (three replicates per test were performed excluding CT flavor where two replicates were done). CMD was very similar ranging from 110 to 117 nm across all the tests performed (GSD was 1.7 for all tests). Average MMAD calculated from the DMS500 data varied in the range from 278 to 287 nm and were comparable with ELPI measured MMAD that varied from 290 to 312 nm.

Similar data obtained from the HPP2 aerosol generation using the same smoking topography (as for the SCS tests) are summarized in Table 2. As one can see aerosol generated by the HPP2 (piston pull–push smoking machine) showed basically a single submicron peak (Figures 7 and S5) and is larger (Figure 8) than the particles generated by the SCS (straight sample deliver type smoking machine). HPP2 generated CMD was in the range from 225 to 259 nm and calculated average MMAD varied from 365 to 410 nm. Comparison with ELPI data showed good agreement between ELPI and DMS500 data, the ELPI average MMAD varied from 368 to 389 nm. Average aerosol mass per puff collected by ELPI across all tests using SCS was 2(±0.3) mg/puff whereas average aerosol mass per puff collected by ELPI while applying HPP2 was ~1.4(±0.2) mg/puff. Average aerosol mass generated by a blu e-cig (CT flavor, three replicates) collected on a Cambridge glass-fiber filters using SCS was 3.1(±0.5) mg/puff, and aerosol mass generated by HPP2 was 2.9(±0.2) mg/puff.

At high sample dilution (with an additional 1/500 dilution factor) SCS aerosol, similar to previous work (Mikheev et al. 2016), showed evaporation of the submicron fraction and a single peak of nanoparticles (Figure S6) whereas the HPP2 aerosol transformed from a single submicron peak into multi-peak distribution showing both nanoparticles and submicron fractions (Figure S7).

E-liquid content of the blu e-cigs measured by HNMR

Table 3 shows the average percentage of PG, VG, water, and nicotine measured by HNMR for all blu e-cig liquids tested. As one can see for 5 (out of six) e-liquid flavors PG varies from ~32 to ~41% whereas VG varies from ~49 to ~58%. CT seems to be an outlier with PG ~13% and VG ~73%, and there is also a greater variability between the samples (standard deviation for PG reached ~11%). Water across all samples varied from 8 to 12%, and nicotine was always ~1%.

LC-TOFMS results

Chemical non-targeted analysis conducted by LC-TOFMS of both blue-cig flavors tested (CC and PC) revealed a number of new organic compounds in the e-cig aerosol that were not found in the e-liquid (Table S2). Observed m/z values for these chemicals were in the range from ~200 to ~300, indicating a high likelihood of low- or semi-volatile nature. Many of these compounds were found in both e-cig flavors, but some of them were specific to either CC or PC flavors.

Author Manuscript Author Manuscript Author Manuscript Author Manuscript

TEM/STEM results

Supplementary Figure S8a shows an example of a typical HAADF STEM image of metal nanoparticles collected on ELPI stage #5 (cut-off size ~93 nm) after blu e-cig CC vaping. Nanoparticles of less than 10 nm size were detected. Elemental EDX mapping of the area indicated that the nanoparticles are copper (Figure S8b). Similar results were obtained for another flavor (PC) tested (Colijn et al. 2018).

Discussion

Analysis of the aerosol size distribution (flow rate influence)

A puffing flow rate increase differently affected measured nanoparticles and submicron fractions. As it was previously discussed (Mikheev et al. 2016) submicron particles are formed as a result of binary nucleation (Stauffer 1976) of the main e-liquid components (PG and VG). For all blu e-cigs tested a flow rate increase from 15 to 35 mL/s brought more vapor from the heated wick to the cooling zone creating higher supersaturation and therefore resulted in a higher aerosol formation (nucleation) rate (Stauffer 1976; Oxtoby 1992) that led to the higher particle number concentration (Figure 2a). Newly formed particles are growing (Vesala et al. 1997) in a surrounding PG/VG vapor while traveling through the aerosol delivery channel, and increased puffing flow rate provides less aerosol growth residence time resulting in particle size decrease (Figure 2b). Another factor that may also play role: a heating element cooling effect could happen due to enhanced ventilation at a high flow rate and it would also reduce vaporizing efficiency. Once a 45 mL/s flow rate was reached blu e-cig aerosol formation rate was either no longer increasing or even started to drop, perhaps due to lack of e-liquid wick supply (at some point the wick drying rate equalized or exceeded the e-liquid supply rate) that resulted in reduced vapor concentration. For one of the tested refillable e-cigs (iTaste VTR) submicron particle concentrations started to decrease even at 25 mL/s flow rate whereas for another refillable e-cig (iTaste SVD) aerosol concentration was still growing at 45 mL/s (Figure 3). The particle size of the submicron fraction gradually decreased as the flow rate increased for all types of tested e-cigs (Figures 3 and 5). A similar trend was recently observed by measuring e-cig particle size using an advanced optical scattering method (Dunkhorst et al. 2018) while varying flow rate from 12.8 through 54.2 mL/s.

Unlike submicron aerosol, the nanoparticles concentration was steadily growing as the puffing flow rate increased from 15 to 45 mL/s and in most cases reached the concentration level of the submicron particles (Figures 2 and 3). Looking at the aerosol spectrum evolution at a 15 mL/s flow rate one can see a very distinct bi-modal distribution similar as earlier reported (Mikheev et al. 2016): a nanoparticle spike at the beginning of the puff followed by the main steady plume of submicron particles (Figures 4–6). At higher flow rates the nanoparticle spike increased and further increase of a flow rate resulted in a continuous growth of nanoparticles through the entire 5 s of a puff duration. At the same time flow rate growth destabilized the submicron fraction—particle concentration goes up and down during the puff development and entire particle size distribution becomes more complicated showing three modes (instead of two modes observed at 15 mL/s). Apparently at a flow rate

Author Manuscript Author Manuscript Author Manuscript Author Manuscript

higher than 15 mL/s none of the studied e-cigs can deliver stable aerosol with a steady particle size distribution throughout the 5 s puff duration.

One of the refillable e-cigs with adjustable power control (box-shaped), the iTaste VTR, showed nanoparticle concentration prevalence over submicron particles starting from the low flow rate and continuing through further flow rate increases (Figures 3 and 6). The iTaste VTR has a heating coil located at ~4 cm from the aerosol exit whereas iTaste SVD e-cig has a heating coil at ~5 cm from the e-cig outlet. A close proximity to the aerosol exit along with a narrowing (down to ~1 mm) diameter of the iTaste VTR aerosol delivery channel (as opposed to iTaste SVD aerosol delivery constant channel diameter ~4 mm) provides shorter time for aerosol growth. Based on the submicron particle concentration measurements we may also assume that wick wetting efficiency is poor for the iTaste VTR and much better for the iTaste SVD.

Due to the complex geometry of the heating element and vapor transition (from heating to cooling) zone of the commercially available e-cigs, an unknown heating temperature, as well as an undefined efficiency of wick saturation by e-liquid, it is not possible to provide accurate calculations of the aerosol formation rate (as well as of the condensational growth of the newly formed particles). Nevertheless, some thoughts provided below might be useful to explain the complicated behavior of e-cig aerosol.

In general, while elevated flow rates decreased submicron fraction aerosol size, nanoparticle size remained unchanged across the entire range of the puffing flow rates. As reported in a previously published work (Mikheev et al. 2016) conducted using the same (blu) brand e-cigs nanoparticles are stable to evaporation even at extremely high dilution (Figure S6) indicating that these nanoparticles should consist of low volatile compounds. It was assumed that (Mikheev et al. 2016) nanoparticles could be generated directly from the heated metal wire (Khan et al. 2014) and in addition to the inductively coupled plasma mass spectrometry measurements (Mikheev et al. 2016) our recent TEM/STEM analysis (Colijn et al. 2018) showed metal nanoparticles collected on ELPI stages (Figure S8). Another source of nanoparticles could be the low- or semi-volatile compounds formed as a result of catalytic heating of the main components of e-liquid as well as residual glycerol that was not fully evaporated even at extremely high dilution. Normally researchers are focused on PG/VG heating reactions that result in formation of the well-known volatile toxicants such as carbonyls (Bekki et al. 2014; Goniewicz et al. 2014; Hutzler et al. 2014; Kosmider et al. 2014; Tayyarah and Long 2014; Jensen et al. 2015; Geiss, Bianchi, and Barrero-Moreno 2016; Khlystov and Samburova 2016; Sleiman et al. 2016; Ogunwale et al. 2017) but low- or semi-volatile compounds that also could be formed during the heating process remained uninvestigated. The newly formed low-volatile (or semivolatile) organic compounds in the e-cig aerosol were detected by the LC-TOFMS (Table S2) and therefore could also contribute to nanoparticle formation (although the chemical nature of these compounds at that moment has not been identified).

Appearance of the third mode in the aerosol spectrums (Figures 6–8) indicates that at elevated flow rate PG and VG may nucleate separately as opposed to binary PG/VG nucleation responsible for the main PG/VG plume of submicron particles. As it was already

Author Manuscript Author Manuscript Author Manuscript Author Manuscript

mentioned due to the complex e-cig geometry it's hard to calculate vapor concentration, temperature, supersaturation, and nucleation rate profiles as it was done in the laminar flow tube reactor (Mikheev et al. 2000, 2002), so we may just assume that at high flow rates PG and VG vapors are not uniformly mixed and critical supersaturation levels for both components could be reached separately therefore creating two independent particle formation sources.

Analysis of the aerosol size distribution (smoking machine influence)

The SCS (straight sample delivery smoking machine) showed smaller particle size than the HPP2 (sample pull–push smoking machine) but the aerosol mass collected on impactor stages generated by SCS was higher than by HPP2. The HPP2 adds an additional 5 s of sample residence time providing particles more time to grow and coagulate, and longer residence time also increases aerosol loss on the walls. Due to high diffusion nanoparticles are more sensitive to wall losses (Willeke and Baron 1993) and also could be absorbed by submicron aerosol, therefore a single submicron peak was observed for the HPP2 aerosol generated at low dilution. At high dilution (as it was already mentioned in "Results" section) HPP2 aerosol transformed into a multi-peak distribution (submicron particles partially evaporated and peaks of nanoparticles appeared). For practical purposes researchers should be aware that the type of smoking machine used to generate e-cig aerosol influences physical properties of the aerosol (size and concentration), whether it also affects chemical properties (like for instance PG/VG ratio) of the aerosol still requires investigation.

Analysis of the aerosol size distribution (DMS500 vs ELPI)

It is interesting that although in general DMS500 measurements showed comparable results with ELPI data, the SCS generated aerosol measured by electrical mobility (DMS500) showed particle size slightly smaller than the aerodynamic (impactor based) data obtained by ELPI. For the HPP2 generated aerosol DMS500 and ELPI particle size data showed tighter agreement. We assume that a possible explanation could be an additional (although very moderate) sample dilution inside the DMS500 (charger flow and classifier sheath flow may add a dilution factor of ~5) that could enhance particle evaporation. On the other hand, pressure inside the DMS500 is higher than in the ELPI (250 mbar vs 40 mbar respectively) therefore particle evaporation inside the DMS500 should be less than inside the ELPI. Also, during the entire sampling session (5 s puff duration and 1 min inter-puff interval per each puff) aerosol collected on ELPI stages was under continuous exposure to the 10 L/min HEPA filtered airflow (10 L/min is an ELPI sampling flow rate). It may cause additional evaporation of the volatile and relatively volatile compounds (water and PG) from the impactor stages and together with the reduced pressure inside the impactor may influence ELPI data (mostly smaller particles should be affected since their travel distance and hence residence time inside the impactor are longer than for the larger particles, their higher surface to volume ratio enhances evaporation, and a pressure drop increases towards the end of the impactor column where the smallest particles are captured). Due to the inherent difference between the electrical mobility classifier column and the inertial impactor design, larger particles inside the DMS500 have longer residence time (as opposed to the ELPI) and therefore have more time to evaporate than the smaller particles.

Author Manuscript Author Manuscript Author Manuscript Author Manuscript

Aged aerosol generated by the HPP2 is less sensitive to evaporation under moderate dilution as was shown by DMS500 vs ELPI data comparison. The evaporative effect should be also dependent upon e-liquid composition and PG/VG ratio. PG has higher volatility than VG and therefore a higher content of PG should lead to higher evaporative losses. In our earlier study (Mikheev et al. 2016) blu e-cigs that were used had e-liquids based on VG (Crenshaw et al. 2016) whereas blu e-cigs used for the current study in general had comparable PG and VG amounts (therefore higher evaporative losses are expected).

Comparing total aerosol mass collected on the impactor stages vs Cambridge filter data (presented in “Results” section) we assume that partial evaporation of e-cig aerosol may happen mainly due to dilution and reduced pressure inside the impactor. At the same time while analyzing the gravimetric data collected on a glass-fiber Cambridge filter one should take into account that undiluted aerosol/vapor mixture at the exit of the e-cig contains highly saturated vapor that may also deposit on a filter (unlike impactor stages that collect only aerosol phase). This experimental artifact (glass fiber filter material can adsorb gas-phase semi-volatiles that would contribute to the total particulate mass) was noticed in a number of atmospheric sampling studies (Calvert et al. 2002) therefore back calculation results of the aerosol parameters based on the filter gravimetric data should be assessed very cautiously.

Limitations

The major limitation of this study was that due to design characteristics of the both instruments (DMS500 and ELPI) used for the particle size measurements a moderate dilution (a factor ~1/33) was applied to the freshly formed e-cig aerosol that could cause partial evaporation and therefore decrease the particle size. As was previously reported (Mikheev et al. 2016) varying the dilution factor from 1/13 to 1/35 did not significantly affect aerosol size distribution of the blu e-cig. At the same time since a dilution lower than 1/13 was not tested we are not excluding the possibility that undiluted e-cig aerosol size may be larger than reported in this study. Unfortunately, as mentioned in the INTRODUCTION section due to different methods of aerosol measurements, puffing profiles, and e-cig brands it is not possible to conduct a direct comparison between the data obtained by various researchers. Recent data obtained at low (~1/3) dilution using an impactor for similar types of e-cigs (blu Plus + Classic) showed larger particle size (Oldham et al. 2018) but a smaller flow rate (11 mL/s) was used. As was reported in the RESULTS section particle size was increasing as the flow rate decreased but the lowest flow rate tested was 15 mL/s and therefore a direct comparison cannot be applied.

Conclusions

The results of this study clearly showed that both the puffing regimen (puffing flow rate) and the method of aerosol generation (type of the smoking machine used) significantly affected aerosol size of the electronic cigarettes emissions. These observations were confirmed by two independent methods of measurement, namely electrical mobility and inertial impaction. Apparently standard testing protocols are required to make future measurements conducted by different research groups available for direct comparison.

Author Manuscript Author Manuscript Author Manuscript Author Manuscript

A peak of nanoparticles was observed at the beginning of each puff for all e-cigs tested across the entire range of the flow rates (from 15 to 45 mL/s). At elevated flow rates nanoparticle concentrations increased and stayed at high levels through the duration of a puff.

A stable submicron aerosol fraction with steady (not changing over puff duration time) particle size distribution was observed only at low (15 mL/s) flow rate. At elevated flow rates (starting from 25 mL/s and higher) submicron aerosols partially evaporated and showed additional peaks transforming the entire aerosol spectrum from a bi-modal to a tri-modal distribution.

Supplementary Material

Refer to Web version on PubMed Central for supplementary material.

Acknowledgments

The content is solely the responsibility of the authors and does not necessarily represent the official views of the NIH or the Food and Drug Administration. The authors would like to thank Chris Nickolaus at Cambustion Ltd for his extensive consulting on DMS500 nonstandard usage.

Funding

Research reported in this publication was supported by grant number P50CA180523 from the National Cancer Institute and FDA Center for Tobacco Products (CTP) awarded to the University of Maryland.

References

Alderman SL, Song C, Moldoveanu SC, and Cole SK. 2015 Particle size distribution of e-cigarette aerosols and the relationship to Cambridge filter pad collection efficiency. Beitr. Tabakforsch./ Contrib. Tob. Res. 26 (4): 183–190. doi: 10.1515/cttr-2015-0006.

Baassiri M, Talih S, Salman R, Karaoghlanian N, Saleh R, El Hage R, Saliba N, and Shihadeh A. 2017 Clouds and “throat hit”: Effects of liquid composition on nicotine emissions and physical characteristics of electronic cigarette aerosols. Aerosol Sci. Technol. 51 (11): 1231–1239.

Bekki K, Uchiyama S, Ohta K, Inaba Y, Nakagome H, and Kunugita N. 2014 Carbonyl compounds generated from electronic cigarettes. Int. J. Environ. Res. Public Health 11 (11):11192–11200. doi:10.3390/ijerph111111192. [PubMed: 25353061]

Cabot R, Anna K, Yurteri CU, and McAughey J. 2013 Aerosol measurement of e-cigarettes. Poster; 32nd Annual Conference, American Association for Aerosol Research.

Calvert JG, Atkinson R, Becker KH, Kamens RM, Seinfeld JH, Wallington TH, and Yarwood G. 2002 The mechanisms of atmospheric oxidation of the aromatic hydrocarbons. Oxford: Oxford University Press.

Colijn HO, Mikheev VB, and McComb DW. 2018 Microscopy Microanalysis 2018 Meeting (M&M2018).

Crenshaw MD, Tefft ME, Buehler SS, Brinkman MC, Clark PI, and Gordon SM. 2016 Determination of nicotine, glycerol, propylene glycol and water in electronic cigarette fluids using quantitative ^{1}H NMR. Magn. Reson. Chem. 54 (11):901–904. doi:10.1002/mrc.4498. [PubMed: 27495876]

Delnevo CD, Giovenco DP, Steinberg MB, Villanti AC, Pearson JL, Niaura RS, and Abrams DB. 2015 Patterns of electronic cigarette use among adults in the United States. Nicotine Tob. Res. 18 (5):715–719. [PubMed: 26525063]

Dunkhorst W, Lipowicz P, Li W, Hux C, Wang Q, and Koch W. 2018 In-situ characterization of e-cigarette aerosols by 90°-light scattering of polarized light. Aerosol Sci. Technol. 52:1–24. doi:10.1080/02786826.2018.1464646.

Author Manuscript Author Manuscript Author Manuscript Author Manuscript

Farsalinos KE, Gillman G, Poulas K, and Voudris V. 2015 Tobacco-Specific nitrosamines in electronic cigarettes: Comparison between liquid and aerosol levels. Int. J. Environ. Res. Public Health 12 (8):9046–9053. doi: 10.3390/ijerph120809046. [PubMed: 26264016]

Fuchs NA 1964 The mechanics of aerosols. New York: Pergamon.

Fuoco FC, Buonanno G, Stabile L, and Vigo P. 2014 Influential parameters on particle concentration and size distribution in the mainstream of e-cigarettes. Environ. Pollut. 184:523–529. doi: 10.1016/j.envpol.2013.10.010. [PubMed: 24172659]

Geiss O, Bianchi I, and Barrero-Moreno J. 2016 Correlation of volatile carbonyl yields emitted by e-cigarettes with the temperature of the heating coil and the perceived sensorial quality of the generated vapours. Int. J. Hyg. Environ. Health 219 (3):268–277. doi:10.1016/j.ijheh.2016.01.004. [PubMed: 26847410]

Goniewicz ML, Knysak J, Gawron M, Kosmider L, Sobczak A, Kurek J, Prokopowicz A, Jablonska-Czapla M, Rosik-Dulewska C, Havel C, et al. 2014 Levels of selected carcinogens and toxicants in vapour from electronic cigarettes. Tob. Control 23 (2):133–139. doi: 10.1136/tobaccocontrol-2012-050859. [PubMed: 23467656]

Hämeri K, Kulmala M, Krissinel E', and Kodenyov G. 1996 Homogeneous nucleation in a laminar flow diffusion chamber: The operation principles and possibilities for quantitative rate measurements. J. Chem. Phys. 105 (17):7683–7695.

Hatch T, and Choate SP. 1929 Statistical description of the size properties of non uniform particulate substances. J. Frankl. Inst. 207 (3):369–387.

Hinds WC 1982 Aerosol technology: Properties behavior, and measurement of airborne particles, 91–95. New York: John Wiley.

Hutzler C, Paschke M, Kruschinski S, Henkler F, Hahn J, and Luch A. 2014 Chemical hazards present in liquids and vapors of electronic cigarettes. Arch. Toxicol. 88 (7):1295–1308. doi:10.1007/s00204-014-1294-7. [PubMed: 24958024]

Ingebrethsen BJ, Cole SK, and Alderman SL. 2012 Electronic cigarette aerosol particle size distribution measurements. Inhal. Toxicol. 24 (14):976–984. doi: 10.3109/08958378.2012.744781. [PubMed: 23216158]

Jensen RP, Luo W, Pankow JF, Strongin RM, and Peyton DH. 2015 Hidden formaldehyde in e-cigarette aerosols. N. Engl. J. Med. 372 (4):392–394. [PubMed: 25607446]

Jensen RP, Strongin RM, and Peyton DH. 2017 Solvent chemistry in the electronic cigarette reaction vessel. Sci. Rep. 7 (1):42549. doi:10.1038/srep42549. [PubMed: 28195231]

Khan A, Modak P, Joshi M, Khandare P, Koli A, Gupta A, Anand S, and Sapra BK. 2014 Generation of high-concentration nanoparticles using glowing wire technique. J. Nanoparticle Res. 16 (12):2776.

Khlystov A, and Samburova V. 2016 Flavoring compounds dominate toxic aldehyde production during e-cigarette vaping. Environ. Sci. Technol. 50 (23):13080–13085. doi:10.1021/acs.est.6b05145. [PubMed: 27934275]

Korzun T, Lazurko M, Munhenzva I, Barsanti KC, Huang Y, Jensen RP, Escobedo JO, Luo W, Peyton DH, and Strongin RM. 2018 E-Cigarette airflow rate modulates toxicant profiles and can lead to concerning levels of solvent consumption. ACS Omega 3 (1): 30–36. [PubMed: 29399647]

Kosmider L, Sobczak A, Fik M, Knysak J, Zaciera M, Kurek J, and Goniewicz ML. 2014 Carbonyl compounds in electronic cigarette vapors: Effects of nicotine solvent and battery output voltage. Nicotine Tob. Res. 16 (10): 1319–1326. doi: 10.1093/ntr/ntu078. [PubMed: 24832759]

Lerner CA, Sundar IK, Watson RM, Elder A, Jones R, Done D, Kurtzman R, Ossip DJ, Robinson R, McIntosh S, et al. 2015 Environmental health hazards of e-cigarettes and their components: Oxidants and copper in e-cigarette aerosols. Environ. Pollut. 198:100–107. doi: 10.1016/j.envpol.2014.12.033. [PubMed: 25577651]

Manigrasso M, Buonanno G, Fuoco FC, Stabile L, and Avino P. 2015 Aerosol deposition doses in the human respiratory tree of electronic cigarette smokers. Environ. Pollut. 196:257–267. doi:10.1016/j.envpol.2014.10.013. [PubMed: 25463721]

Marini S, Buonanno G, Stabile L, and Ficco G. 2014 Short-term effects of electronic and tobacco cigarettes on exhaled nitric oxide. Toxicol. Appl. Pharmacol. 278 (1): 9–15. doi:10.1016/j.taap.2014.04.004. [PubMed: 24732441]

Author Manuscript Author Manuscript Author Manuscript Author Manuscript

Martonen TB 1992 Deposition patterns of cigarette smoke in human airways. Am. Ind. Hyg. Assoc. J. 53 (1): 6–18. [PubMed: 1590221]

Mikheev VB, Brinkman MC, Granville CA, Gordon SM, and Clark PI. 2016 Real-time measurement of electronic cigarette aerosol size distribution and metals content analysis. Nicotine Tob. Res. 18 (9):1895–1902. [PubMed: 27146638]

Mikheev VB, Irving PM, Laulainen NS, Barlow SE, and Pervukhin VV. 2002 Laboratory measurement of water nucleation using a laminar flow tube reactor. J. Chem. Phys. 116 (24):10772–10786.

Mikheev VB, Laulainen NS, Barlow SE, Knott M, and Ford IJ. 2000 The laminar flow tube reactor as a quantitative tool for nucleation studies: Experimental results and theoretical analysis of homogeneous nucleation of dibutylphthalate. J. Chem. Phys. 113 (9): 3704–3718.

Ogunwale MA, Li M, Ramakrishnam Raju MV, Chen Y, Nantz MH, Conklin DJ, and Fu XA. 2017 Aldehyde detection in electronic cigarette aerosols. ACS Omega 2 (3):1207–1214. doi:10.1021/acsomega.6b00489. [PubMed: 28393137]

Oldham MJ, Zhang J, Rusyniak MJ, Kane DB, and Gardner WP. 2018 Particle size distribution of selected electronic nicotine delivery system products. Food Chem. Toxicol. 113:236–240. [PubMed: 29408542]

Oxtoby DW 1992 Homogeneous nucleation: Theory and experiment. J. Phys.: Condens. Matter 4 (38):7627.

Phalen RF, Oldham MJ, and Schum GM. 2002 The deposition of concentrated cigarette smoke in airway models. Ann. Occup. Hyg. 46 (suppl_1):343–345.

Pratte P, Cosandey S, and Goujon-Ginglinger C. 2016 A scattering methodology for droplet sizing of e-cigarette aerosols. Inhal. Toxicol. 28 (12):537–545. [PubMed: 27644268]

Rossiter WJ Jr, MClure G, Brown PW, and Galuk KG. 1985 An investigation of the degradation of aqueous ethylene glycol and propylene glycol solutions using ion chromatography. Sol. Energy Mater. 11 (5–6): 455–467.

Salamanca JC, Munhenzva I, Escobedo JO, Jensen RP, Shaw A, Campbell R, Luo W, Peyton DH, and Strongin RM. 2017 Formaldehyde hemiacetal sampling, recovery, and quantification from electronic cigarette aerosols. Sci. Rep. 7 (1):11044 [PubMed: 28887552]

Saliba N, Hellani AE, Honein E, Salman R, Zeaiter J, and Shihadeh A. 2018 The catalytic role of the metallic coils of electronic cigarettes in aldehyde formation. 2018 Annual Meeting—Society for Research on Nicotine and Tobacco, Baltimore, MD, USA.

Scungio M, Stabile L, and Buonanno G. 2018 Measurements of electronic cigarette-generated particles for the evaluation of lung cancer risk of active and passive users. J. Aerosol Sci. 115:1–11.

Singh T, Arrazola RA, Corey CG, Husten CG, Neff LJ, Homa DM, and King BA. 2016 Tobacco use among middle and high school students—United States, 2011–2015. MMWR Morb. Mortal. Wkly. Rep. 65 (14): 361. [PubMed: 27077789]

Sleiman M, Logue JM, Montesinos VN, Russell ML, Litter MI, Gundel LA, and Destaillats H. 2016 Emissions from electronic cigarettes: Key parameters affecting the release of harmful chemicals. Environ. Sci. Technol. 50 (17):9644–9651. doi:10.1021/acs.est.6b01741. [PubMed: 27461870]

St. Helen G, Havel C, Dempsey DA, Jacob P III, and Benowitz NL. 2016 Nicotine delivery, retention and pharmacokinetics from various electronic cigarettes. Addiction 111 (3):535–544. [PubMed: 26430813]

Stauffer D 1976 Kinetic theory of two-component (heteromolecular) nucleation and condensation. J. Aerosol Sci. 7 (4):319–333.

Tayyarah R, and Long GA. 2014 Comparison of select analytes in aerosol from e-cigarettes with smoke from conventional cigarettes and with ambient air. Regul. Toxicol. Pharmacol. 70 (3):704–710. doi:10.1016/j.yrtph.2014.10.010. [PubMed: 25444997]

Tuma C, Laino T, Martin E, Stolz S, and Curioni A. 2013 Modeling the impact of solid surfaces in thermal degradation processes. ChemPhysChem 14 (1):88–91. doi: 10.1002/cphc.201200921. [PubMed: 23180393]

Vesala T, Kulmala M, Rudolf R, Vrtala A, and Wagner PE. 1997 Models for condensational growth and evaporation of binary aerosol particles. J. Aerosol Sci. 28 (4):565–598.

Vohra V, and Heist RH. 1996 The flow diffusion nucleation chamber: A quantitative tool for nucleation research. J. Chem. Phys. 104 (1):382–395.

Author Manuscript Author Manuscript Author Manuscript Author Manuscript

Volesky KD, Maki A, Scherf C, Watson LM, Cassol E, and Villeneuve PJ. 2016 Characteristics of e-cigarette users and their perceptions of the benefits, harms and risks of e-cigarette use: Survey results from a convenience sample in Ottawa, Canada. Health Promot. Chronic Dis. Prev. Can. 36 (7):130. [PubMed: 27409988]

Vreeke S, Korzun T, Luo W, Jensen RP, Peyton DH, and Strongin RM. 2018 Dihydroxyacetone levels in electronic cigarettes: Wick temperature and toxin formation. Aerosol Sci. Technol. 52 (4):370–376. [PubMed: 30686853]

Willeke K, and Baron PA. 1993 Aerosol measurement: Principles, Techniques Applications, 105–106. New York: Van Nostrand Reinhold.

Williams M, Villarreal A, Bozhilov K, Lin S, and Talbot P. 2013 Metal and silicate particles including nanoparticles are present in electronic cigarette cartomizer fluid and aerosol. PLoS One 8 (3):e57987. doi:10.1371/journal.pone.0057987. [PubMed: 23526962]

Zhang Y, Sumner W, and Chen DR. 2013 In vitro particle size distributions in electronic and conventional cigarette aerosols suggest comparable deposition patterns. Nicotine Tob. Res. 15 (2):501–508. doi:10.1093/ntr/nts165. [PubMed: 23042984]

Zhao T, Shu S, Guo Q, and Zhu Y. 2016 Effects of design parameters and puff topography on heating coil temperature and mainstream aerosols in electronic cigarettes. Atmos. Environ. 134:61–69. doi:10.1016/j.atmosenv.2016.03.027.

Author Manuscript Author Manuscript Author Manuscript Author Manuscript

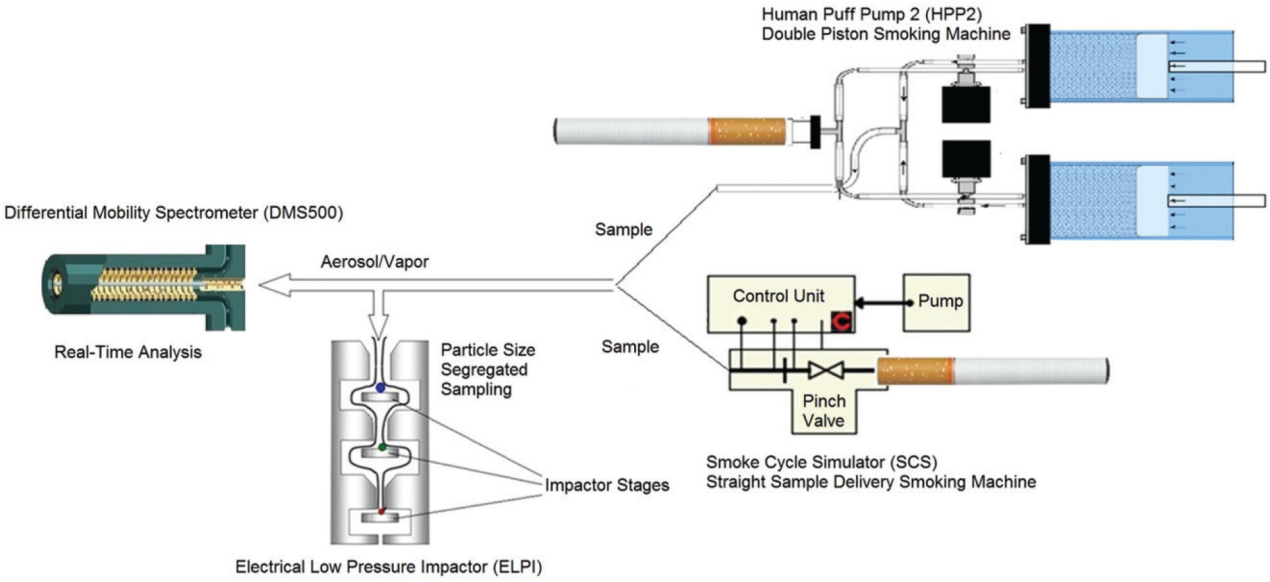

Figure 1.
Experimental setup. DMS500 and ELPI connected to the SCS and HPP2 for simultaneous sampling.

Author Manuscript
Author Manuscript
Author Manuscript
Author Manuscript

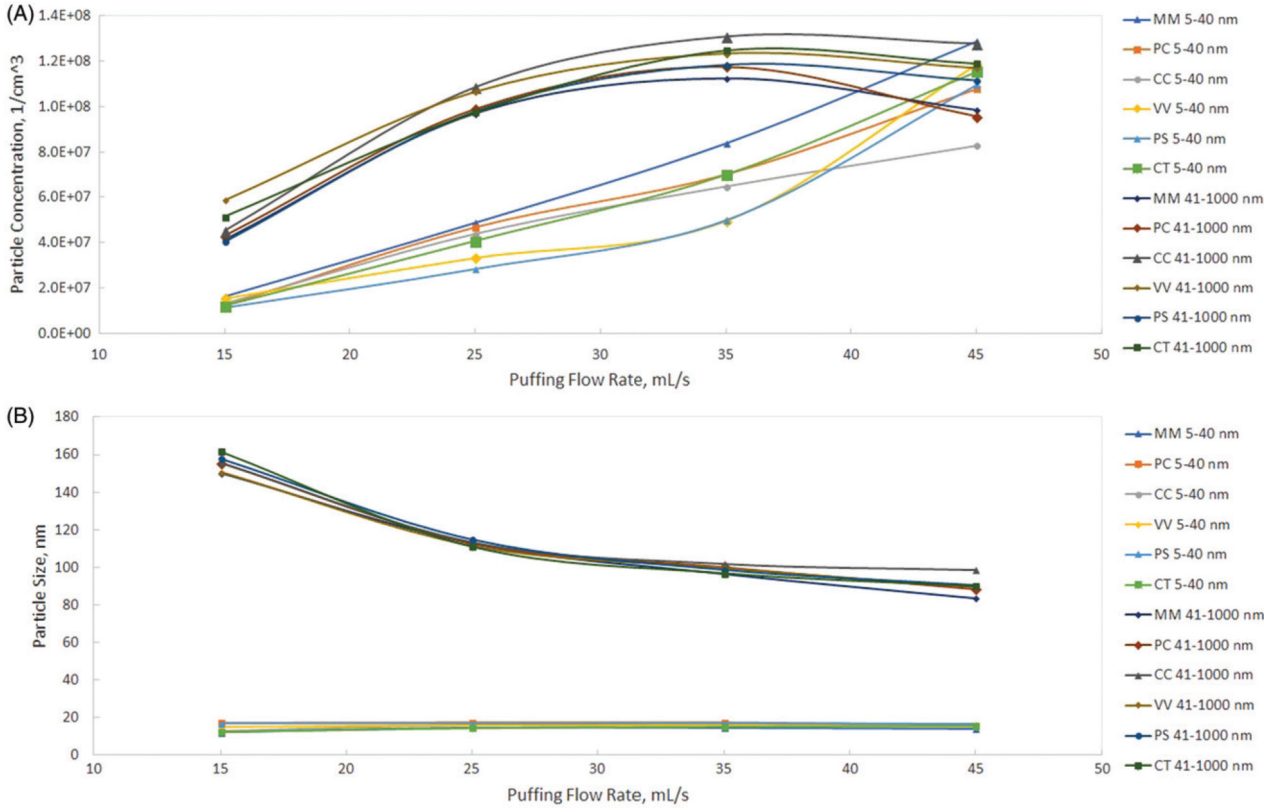

Figure 2.

Particle number concentration (a) and particle size CMD (b) as a function of puffing flow rate. Blu e-cigs.

Author Manuscript
Author Manuscript
Author Manuscript
Author Manuscript

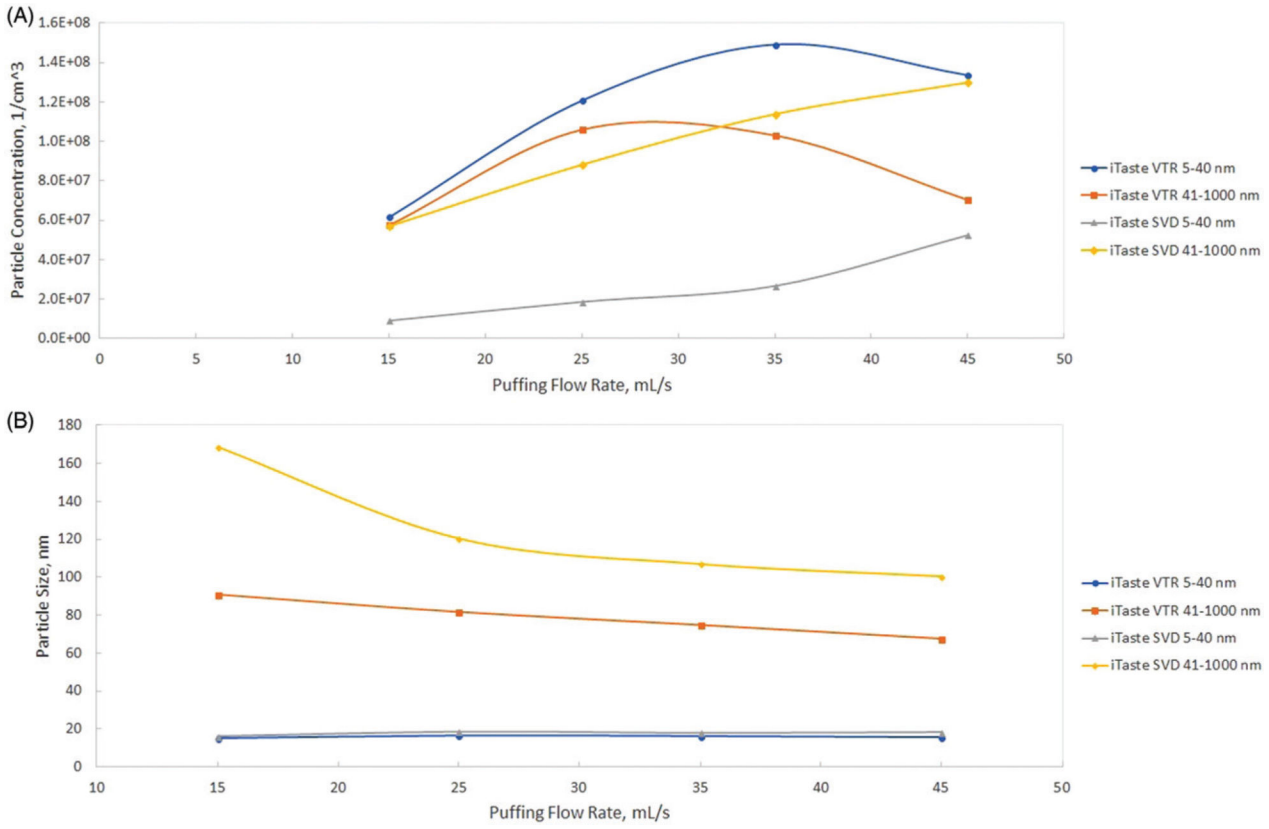

Figure 3.

Particle number concentration (a) and particle size CMD (b) as a function of puffing flow rate. iTaste SVD and iTaste VTR.

Author Manuscript Author Manuscript Author Manuscript Author Manuscript

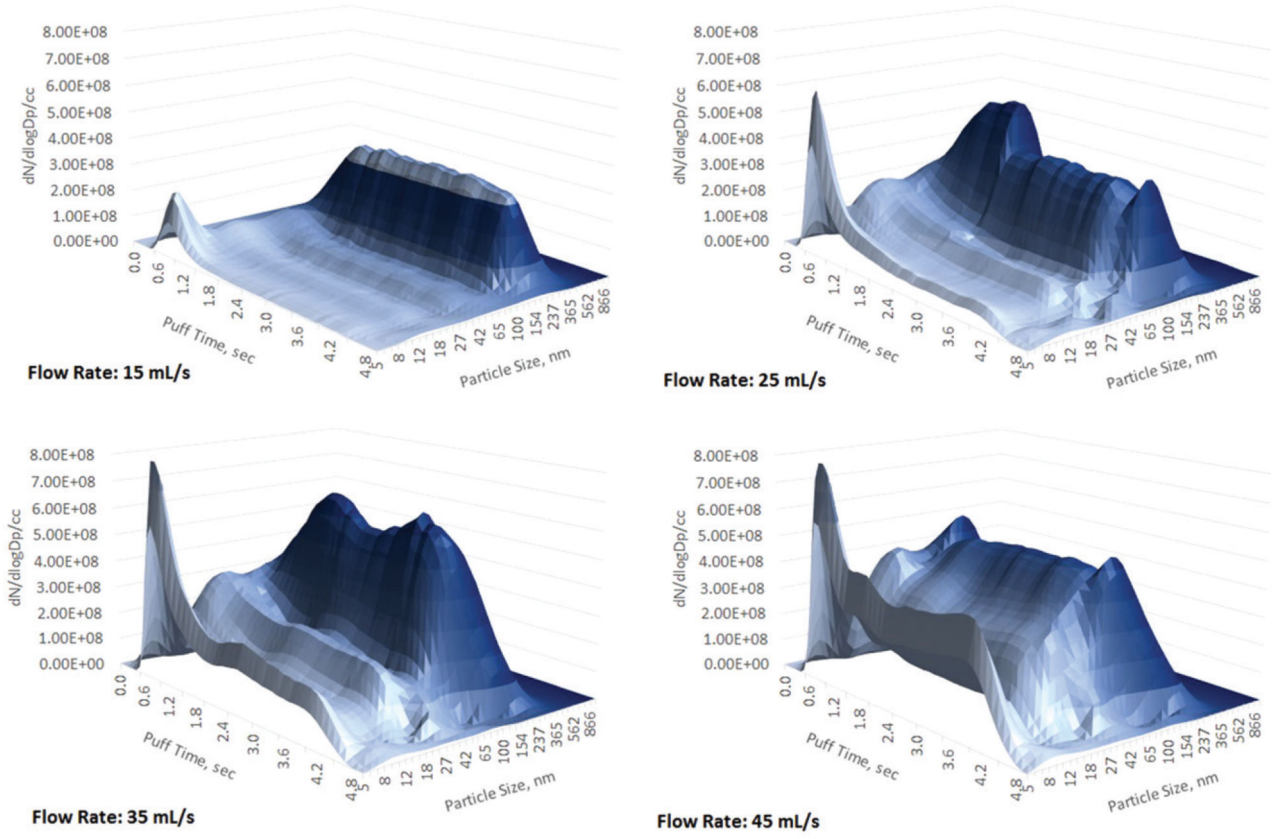

Figure 4.

Aerosol size distribution, blu classic tobacco mid-nicotine. 5 s puff. Flow rates 15, 25, 35, and 45 mL/s.

Author Manuscript Author Manuscript Author Manuscript Author Manuscript

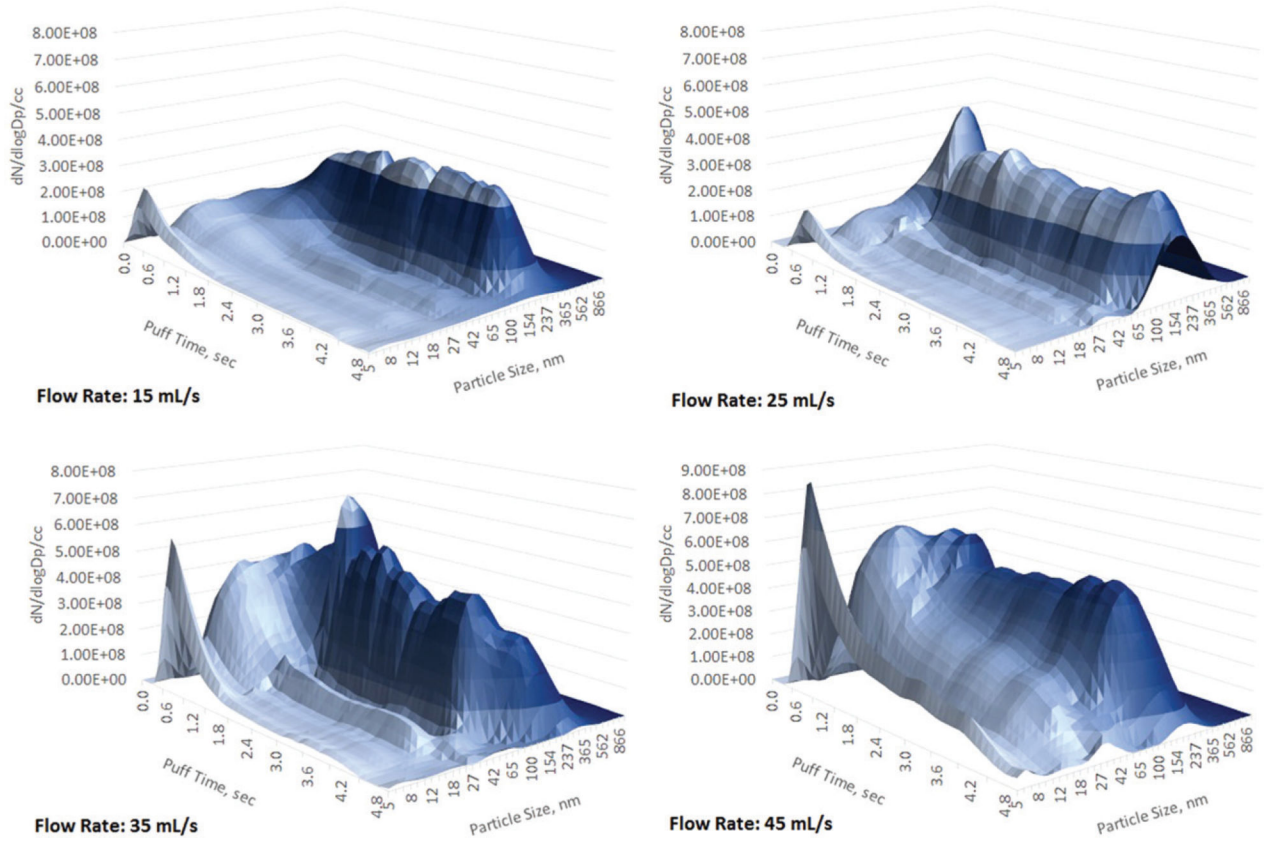

Figure 5.

Aerosol size distribution, iTaste SVD, PG/VG =50/50, 5 V, 1.8 ohm. 5 s puff. Flow rates 15, 25, 35, and 45 mL/s.

Author Manuscript Author Manuscript Author Manuscript Author Manuscript

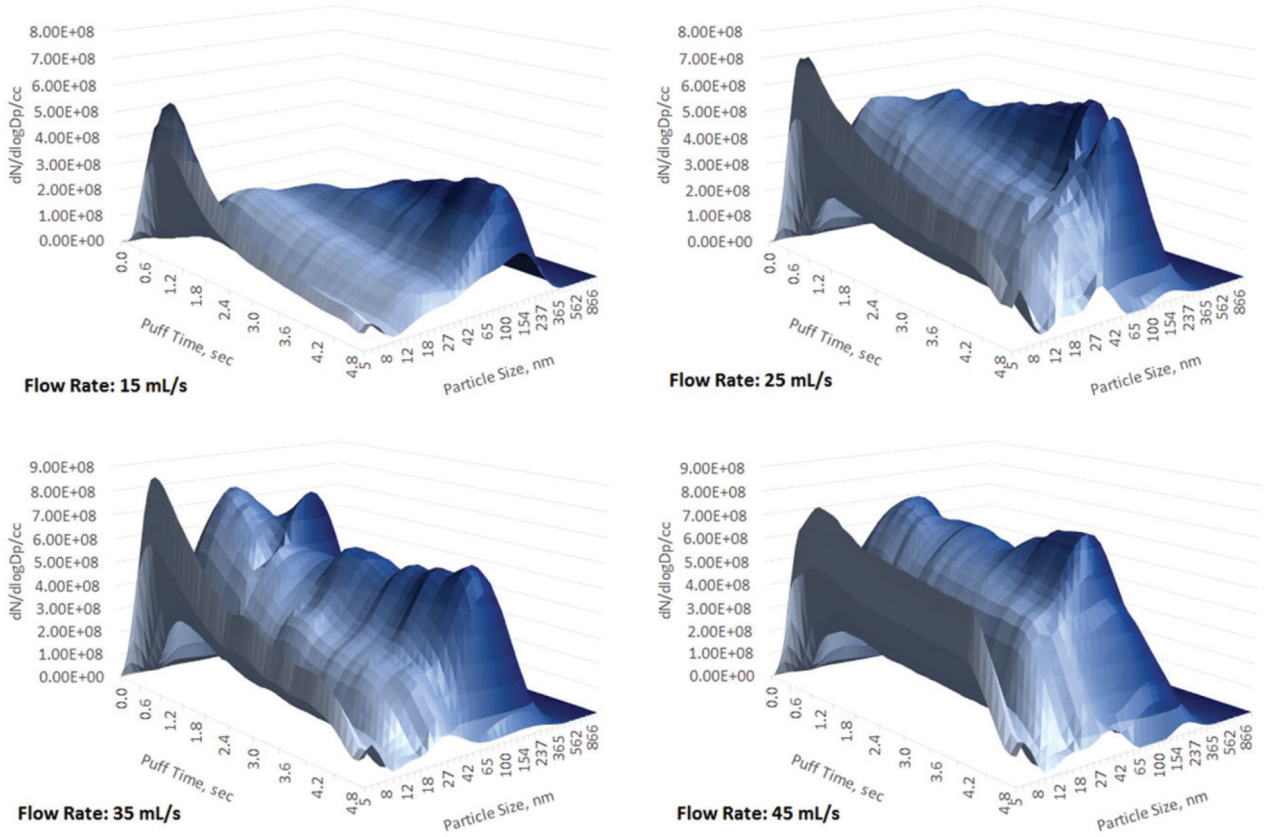

Figure 6.

Aerosol size distribution, iTaste VTR, PG/VG =50/50, 4 V, 2.1 ohm. 5 s puff. Flow rates 15, 25, 35, and 45 mL/s.

Author Manuscript Author Manuscript Author Manuscript Author Manuscript

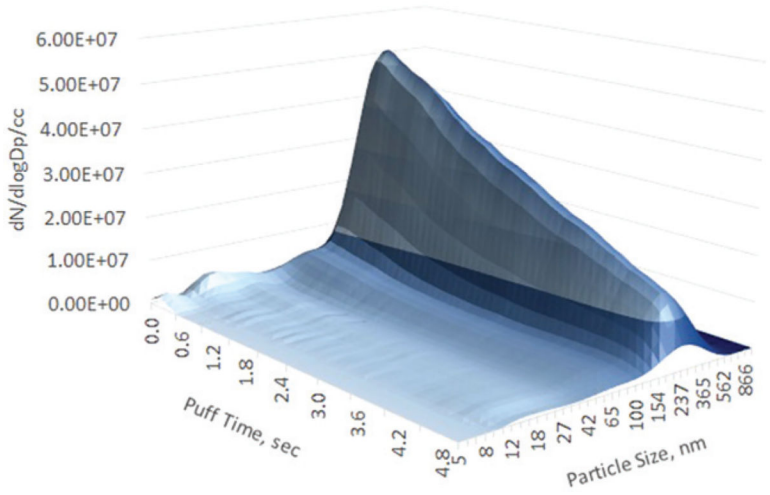

Figure 7.
Aerosol size distribution, HPP2, blu classic tobacco mid-nicotine. 5 s puff. Flow rate 25 mL/s.

Author Manuscript Author Manuscript Author Manuscript Author Manuscript

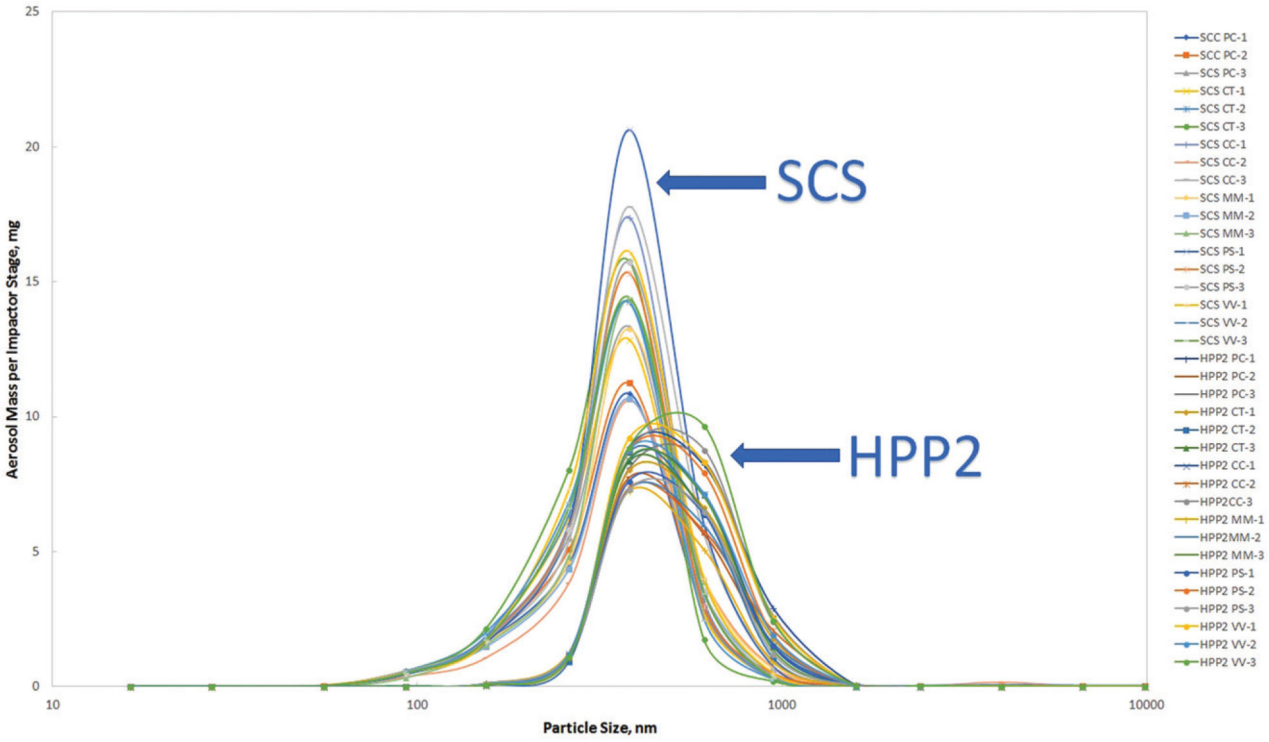

Figure 8.
ELPI data. Particle size mass distribution. SCS vs HPP2. Blu e-cigs. 5 s puff. Flow rate 25 mL/s.

Author Manuscript Author Manuscript Author Manuscript Author Manuscript

Table 1.

Results of the blu e-cigarettes particle size measurements.

	DMS500 measured CMD (GCD)							DMS500 calculated MMAD				ELPI measured MMAD			
SCS Blu e-cig flavor	**CMD nm Test-1**	**GSD**	**CMD nm Test-2**	**GSD**	**CMD nm Test-3**	**GSD**	**Average CMD nm**	**MMAD nm Test-1**	**MMAD nm Test-2**	**MMAD nm Test-3**	**Average MMAD nm**	**MMAD nm Test-1**	**MMAD nm Test-2**	**MMAD nm Test-3**	**Average MMAD nm**
PC	114	1.7	115	1.7	110	1.7	113	285	287	275	282	300	299	299	299
PS	114	1.7	117	1.7	114	1.7	115	285	292	285	287	317	302	304	308
CT	110	1.7	NA	NA	113	1.7	112	275	NA	282	278	294	NA	287	290
MM	112	1.7	112	1.7	114	1.7	113	280	280	285	281	311	307	310	309
CC	113	1.7	113	1.7	115	1.7	114	282	282	287	284	303	317	317	312
VV	113	1.7	112	1.7	111	1.7	112	282	280	277	280	301	293	299	298

DMS500 vs ELPI data. Aerosol generated using SCS.

Aerosol Sci Technol. Author manuscript; available in PMC 2020 August 06.

Author Manuscript Author Manuscript Author Manuscript Author Manuscript

Table 2.

Results of the blu e-cigarettes particle size measurements.

	DMS500 measured CMD (GCD)							DMS500 calculated MMAD				ELPI measured MMAD			
SCS Blu e-cig flavor	**CMD nm Test-1**	**GSD**	**CMD nm Test-2**	**GSD**	**CMD nm Test-3**	**GSD**	**Average CMD nm**	**MMAD nm Test-1**	**MMAD nm Test-2**	**MMAD nm Test-3**	**Average MMAD nm**	**MMAD nm Test-1**	**MMAD nm Test-2**	**MMAD nm Test-3**	**Average MMAD nm**
PC	259	1.5	236	1.5	239	1.5	244	433	389	393	405	393	366	393	384
PS	230	1.4	244	1.4	228	1.4	234	362	391	364	372	373	380	374	375
CT	252	1.5	254	1.4	241	1.4	249	409	NA	385	397	375	365	369	370
MM	225	1.4	232	1.4	232	1.4	229	359	364	371	365	359	374	372	368
CC	235	1.4	242	1.5	250	1.5	242	375	399	406	393	373	375	397	381
VV	255	1.5	243	1.5	256	1.5	251	414	394	422	410	388	373	406	389

DMS500 vs ELPI data. Aerosol generated using HPP2.

Author Manuscript Author Manuscript Author Manuscript Author Manuscript

Table 3.

Main components of the blu e-cig e-liquid measured by HNMR, %(±StDev).

Flavor	CC	PC	CT	VV	MM	PS
PG	40.35 (±1.45)	41.41 (±0.09)	13.31 (±10.85)	36.03 (±0.17)	35.99 (±0.21)	32.38 (±0.37)
VG	49.54 (±0.92)	48.72 (±0.18)	73.51 (±7.69)	54.73 (±0.36)	53.48 (±1.74)	58.30 (±0.31)
Water	9.11 (±0.50)	8.80 (±0.08)	12.16 (±3.17)	8.13 (±0.42)	9.50 (±1.62)	8.25 (±0.06)
Nicotine	0.99 (±0.03)	1.07 (±0.02)	1.02 (±0.01)	1.10 (±0.00)	1.03 (±0.09)	1.08 (±0.02)

N = 3 (except for CC and PC where *N* = 2).

Aerosol Sci Technol. Author manuscript; available in PMC 2020 August 06.